

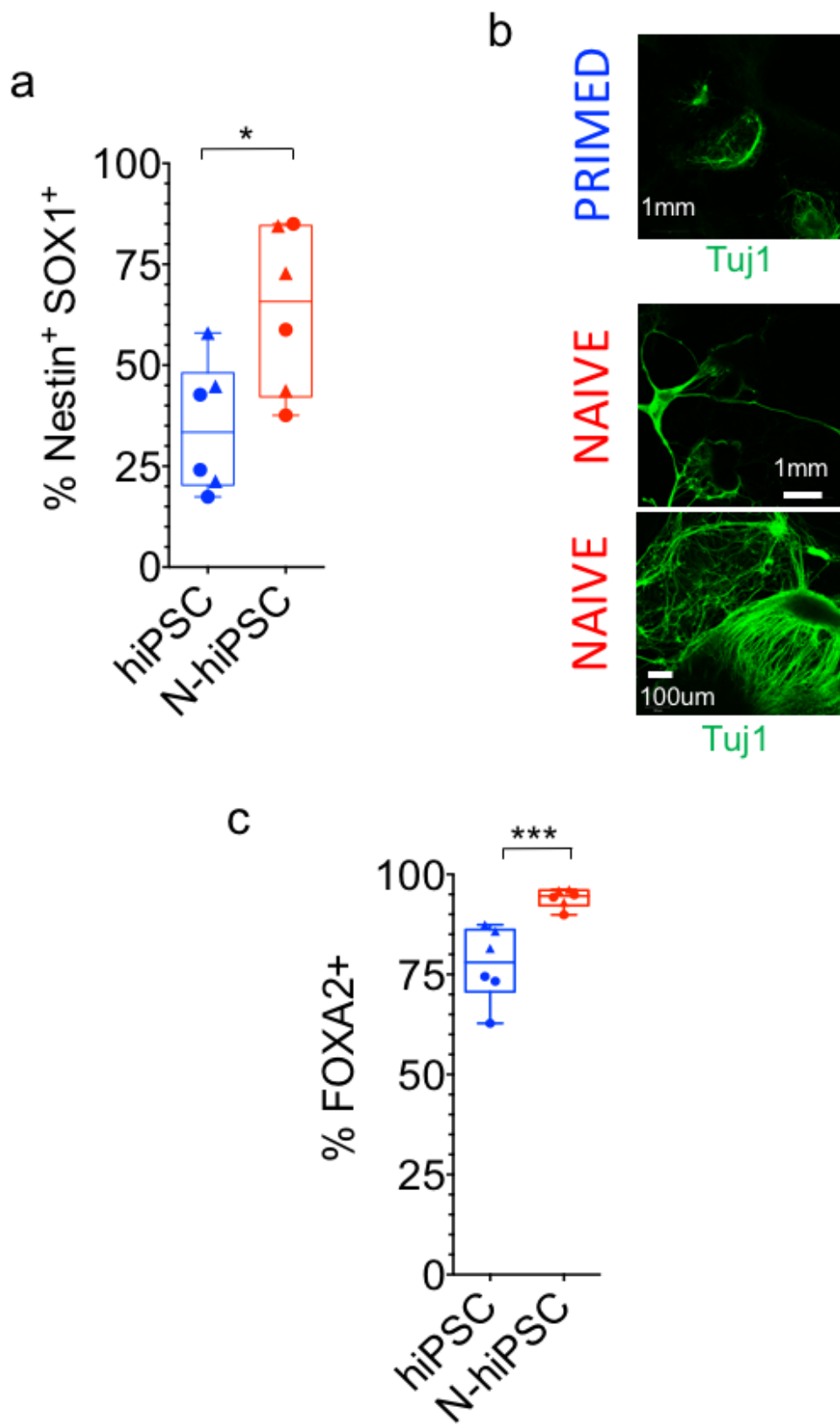
SUPPLEMENTARY INFORMATION

**Vascular Progenitors Generated from Tankyrase Inhibitor-Regulated Naïve
Diabetic Human iPSC Potentiate Efficient Revascularization of Ischemic Retina**

Park *et. al*

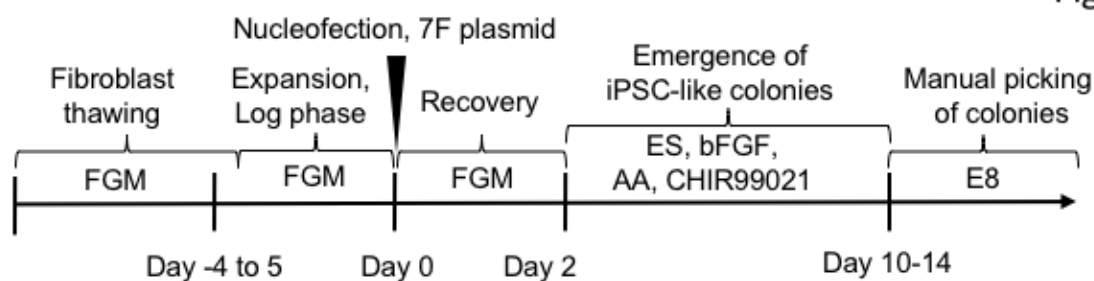
Supplementary Figures

Supplementary Figure 1. *In vitro* multi-lineage directed differentiations of paired isogenic primed vs. naïve normal (non-diabetic) hiPSC lines. Isogenic primed (E8 cultures) vs. naïve-reverted (LIF-3i cultures) hiPSC were differentiated in parallel using established multi-lineage protocols and commercially available kits, as previously described and without any requirement for re-priming ^{12,13}. Shown are direct comparisons between normal (non-diabetic) isogenic hiPSC lines demonstrating augmented differentiation capacities to all three germ layers and robust/improved capacity for terminal differentiation. **(a)** Neuro-ectodermal differentiation of isogenic comparisons of primed vs. naïve hPSC lines performed as described with PSC neural induction medium ¹² (Thermo Fisher Scientific; $n=6$, three normal fibroblast-hiPSC lines (circles; C1.2, C2, 7ta) and three normal cord blood (CB)-derived hiPSC lines (triangles; E5C3, E5C1, LZ6+10); see **Table S1**). Shown are flow cytometry analysis of differentiation cultures for protein expressions of % Nestin⁺SOX1⁺ neural progenitor cells determined by flow cytometry at day 10 neural differentiation, as described ^{12,13}. **(b)** Representative images of Tuj1-expressing terminally-differentiated cells from a primed (E8 culture) vs naïve (LIF-3i culture) CB-iPSC line (E5C3) after 5 weeks of neural differentiation, performed as described ^{12,13}, and demonstrating higher incidence of extended Tuj1⁺ neurites elongated over 3 mm in N-CB-iPSC relative to primed CB-iPSC. **(c)** Definitive endodermal differentiation of isogenic primed vs naïve-hiPSC ($n=6$; hiPSC lines as above (**Table S1**), each individual line represented by a different color, with mean and SEM shown). Differentiations were performed as described with STEMdiff definitive endoderm kit and STEMdiff APEL medium (StemCell Technologies) ¹². Shown are % differentiated cells expressing FOXA2⁺ endodermal progenitor cells.

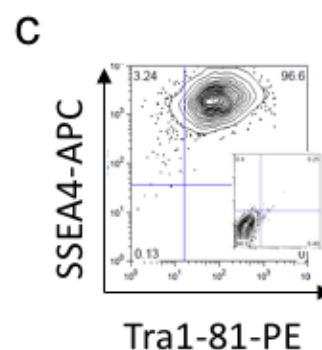
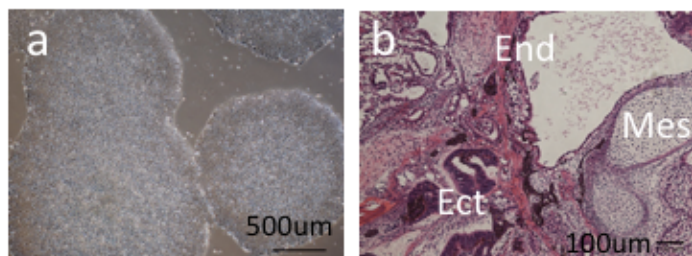


Supplementary Figure 2. Non-integrated episomal reprogramming of type I diabetic skin fibroblasts into conventional DhiPSC lines, and subsequent naïve reversion into N-DhiPSC with the LIF-3i culture system. (a) Scheme of timeline of reprogramming of diabetic skin fibroblasts for the generation of conventional, primed DhiPSC. FGM: fibroblast growth medium, ES: ES medium, AA: ascorbic acid, CHIR99021: GSK3- β inhibitor, E8: essential 8 medium. (b^a) typical morphology of conventional primed DhiPSC cultured in E8 medium on vitronectin-coated plates. (b^b) teratoma formation in NOG mice from primed DhiPSC line (E1CA1) generated well-developed three germ layer organoid structures. (c) Flow cytometry analysis of conventional DhiPSC lines demonstrated >95% SSEA4⁺TRA1-81⁺ expressions. (d) Scheme of timeline of naïve reversion (LIF-5i/LIF-3i) of primed, conventional DhiPSC into N-DhiPSC, performed as described ¹². (e) typical dome-shaped colonies (left, ^{a,c}) in LIF-3i naïve cultures of N-DhiPSC lines (E1C1, E1CA2 – see **Table S1**) and their normal G-banded karyotypes (right, ^{b,d}) following 3-10 passages in naïve (LIF-3i) conditions. (f) Representative teratoma H&E sections from two N-DhiPSC lines (E1CA2 and E1C1). Shown are ectodermal neural rosette (Ect), endodermal epithelial gut (End), and mesodermal cartilage (Meso) structures. Scale bar = 100 μ m.

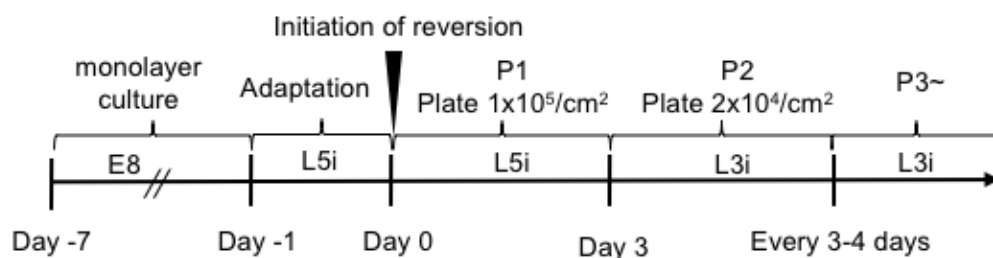
a Generation of Conventional Primed DhiPSC



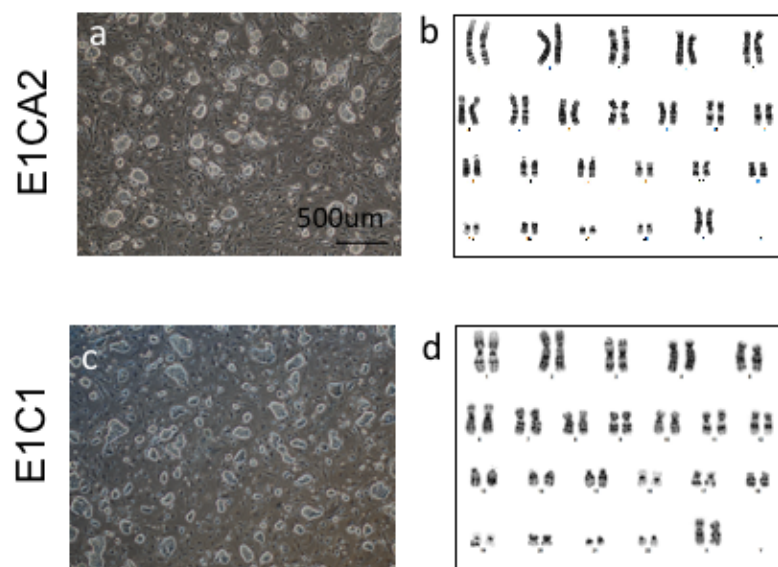
b DhiPSC



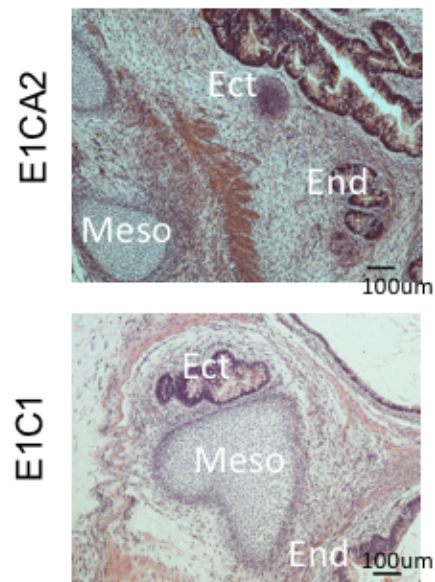
d LIF-3i Naive Reversion of Conventional DhiPSC



e N-DhiPSC lines



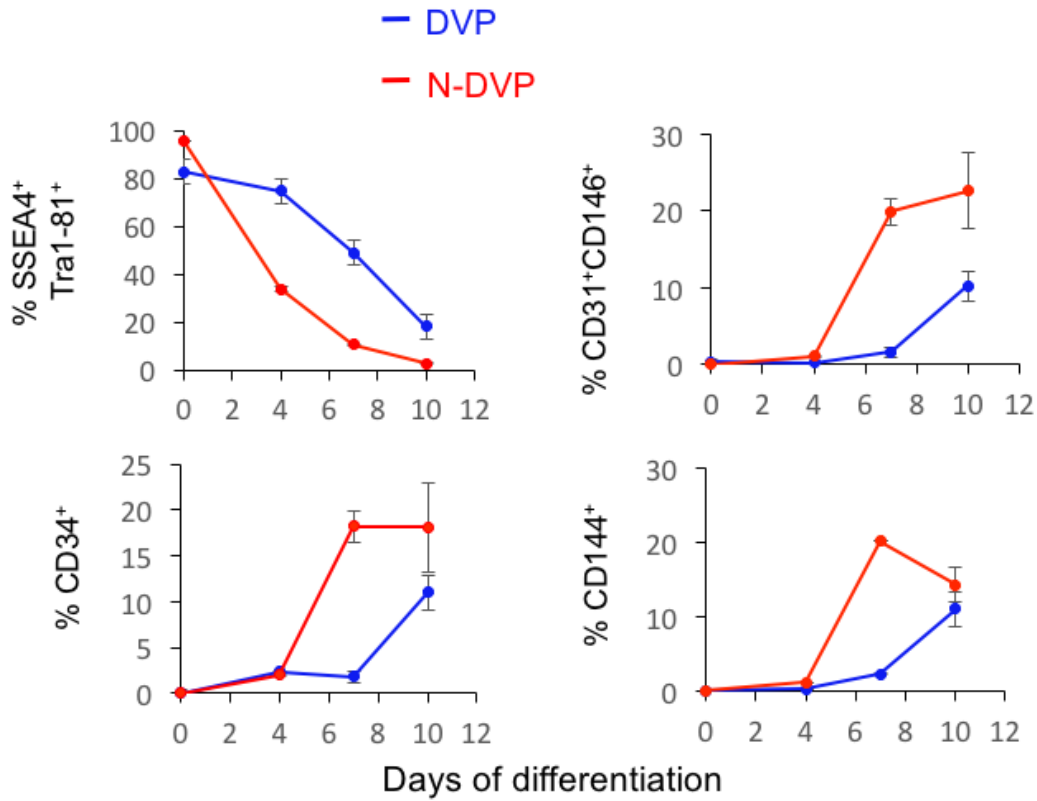
f N-DhiPSC lines



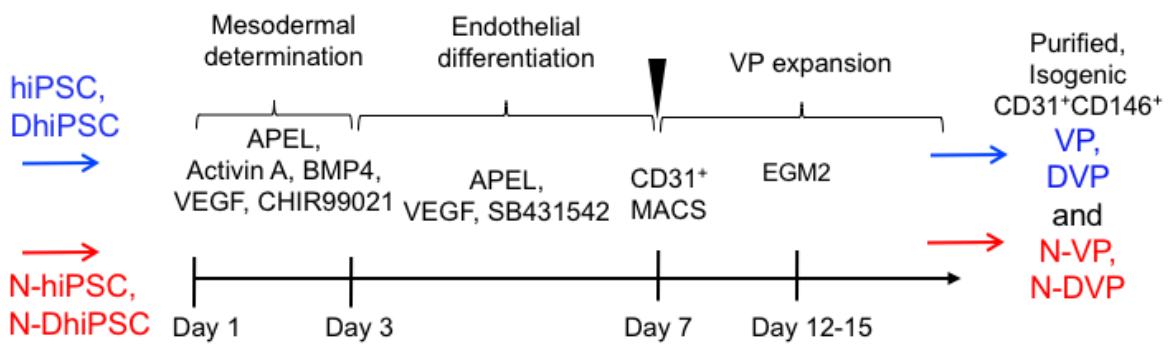
Supplementary Figure 3. APEL vascular differentiation system. (a) Kinetics patterns of surface protein expressions by flow cytometry during APEL vascular differentiation for pluripotency markers (SSEA4, TRA-1-81) and vascular markers (CD31, CD146, CD34, CD144) from isogenic primed (blue) and naïve (red) DhiPSC lines. Shown are mean results with SEM of two independent differentiation experiments of N-DhiPSC and their isogenic primed DhiPSC counterparts (lines E1C1, E1CA1; $n=2$). (b) Shown are indicated growth factors and inhibitor molecules, as described in Methods. Differentiation cultures were enriched for CD31-expressing VP using magnetic-activated cell sorting (MACS); CD31⁺ VP co-express CD146 post-MACS enrichment. These CD31⁺CD146⁺ VP populations were further expanded for several passages in EGM2 medium prior to *in vitro* characterization or injection into I/R-injured murine NOG eyes.

Supplementary Fig. 3

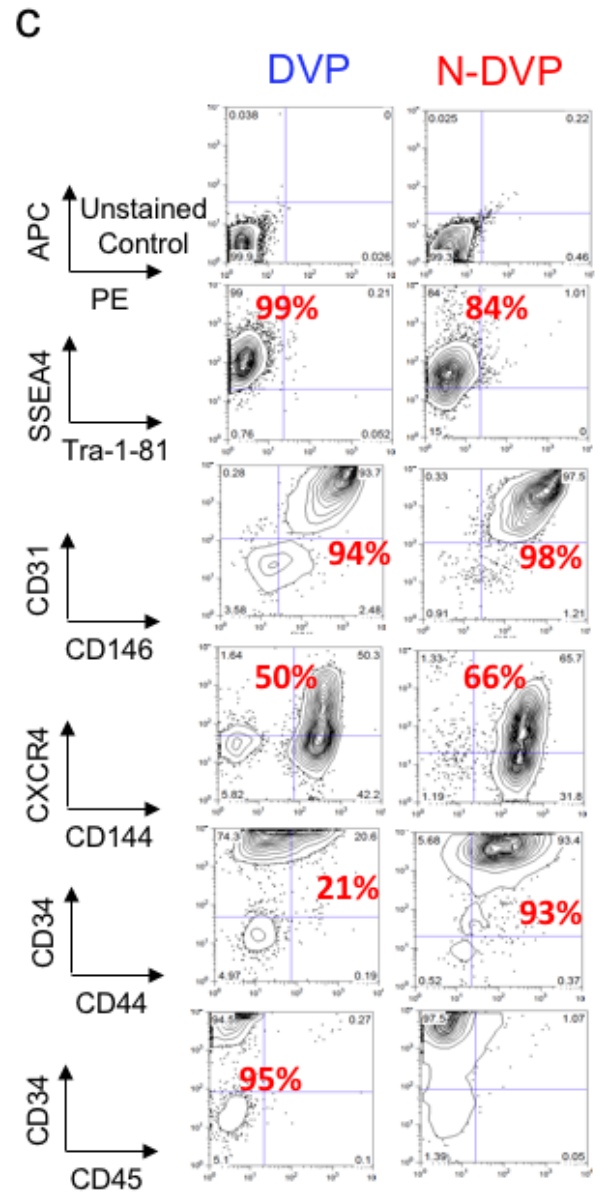
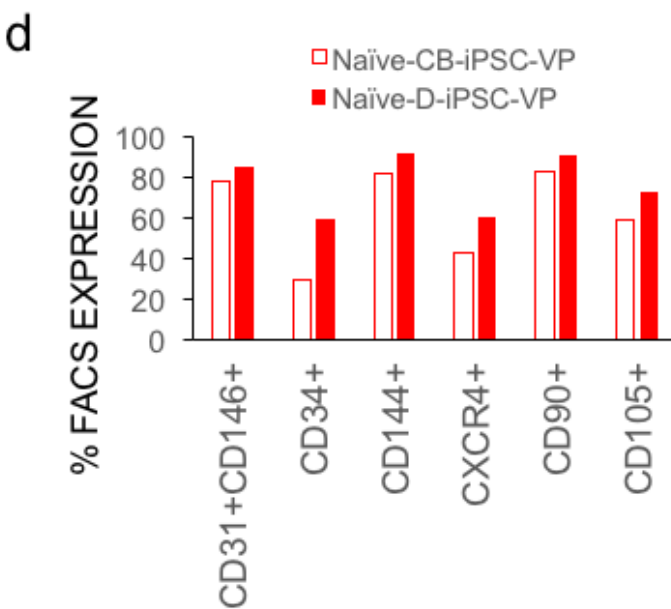
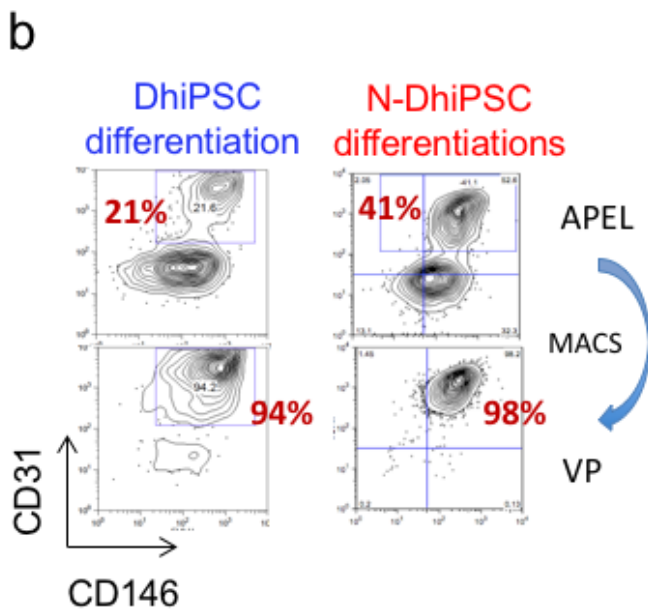
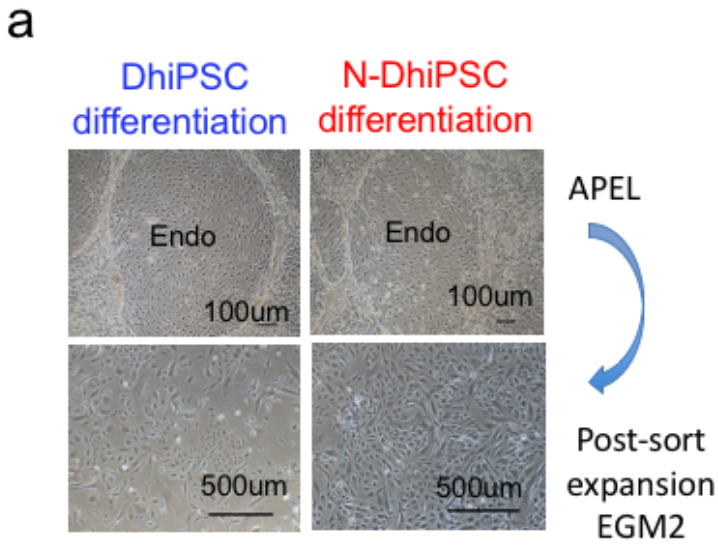
a



b

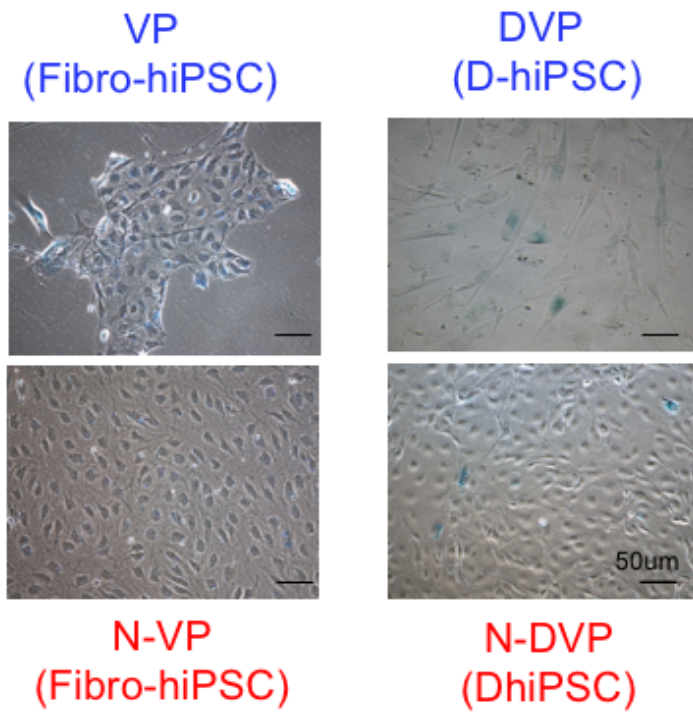


Supplementary Figure 4. APEL vascular differentiation of primed and naïve DhiPSC and FACS gating strategy for CD31⁺CD146⁺ VP purifications. (a) Both primed (E8) and naïve (LIF-3i) DhiPSC (line E1C1) differentiated efficiently using the APEL monolayer vascular differentiation system. Shown are morphologies of APEL-differentiated DVP cells before and after CD31-sorting and re-plating in EGM2. (b) Representative flow cytometry expressions of CD31 and CD146 prior to and post sorting of APEL differentiation cultures with CD31 magnetic bead-tagged antibody (MACS: magnetic activated cell sorting). (c) Flow cytometry analysis post CD31-sort (prior to EGM2 expansion) vascular lineage surface marker analysis of primed DVP (left panel) vs N-DVP (right panel) demonstrating no significant differences in vascular marker expressions post CD31-sorting from APEL cultures. (d) CD31⁺CD146⁺ N-VP and N-DVP were generated from normal non-diabetic naïve N-CBiPSC and naïve N-DhiPSC, respectively, and analyzed post-CD31 sorting for surface expressions of vascular markers (e.g., CD31, CD146, CD144, CXCR4, CD90, and CD105); which demonstrated no significant differences.

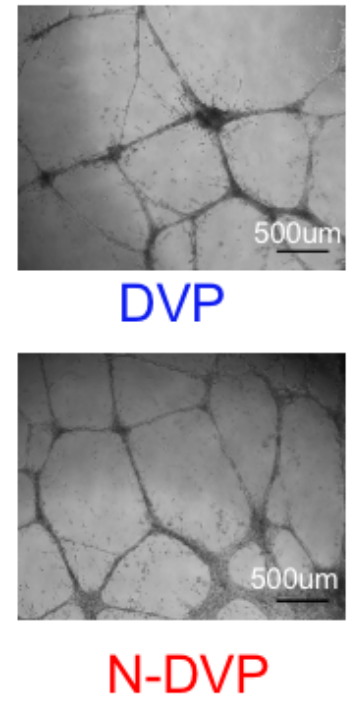


Supplementary Figure 5. *In vitro* vascular function of DVP vs. N-DVP. (a) Representative images of β -galactosidase senescence assays at passage 4 post re-plating of primed VP vs. N-VP from a normal fibroblast-hiPSC (C1.2), and primed DVP vs N-DVP from a diabetic hiPSC line (E1C1). (b) Matrigel vascular tube formation assay demonstrated that N-DVP formed longer and more mature types of tubes than primed DVP. (c) (Left panel) representative flow cytometry analysis of EdU assays at passage 1 and passage 3 post re-plating of primed DVP vs. N-DVP from a diabetic hiPSC line (E1C1) (see **Figure 4e**). (Right panel) EdU proliferation assays of purified DVP after 1-5 passages in EGM2 post-CD31⁺ purification. DhiPSC line E1CA2; $n=2$ independent experiments.

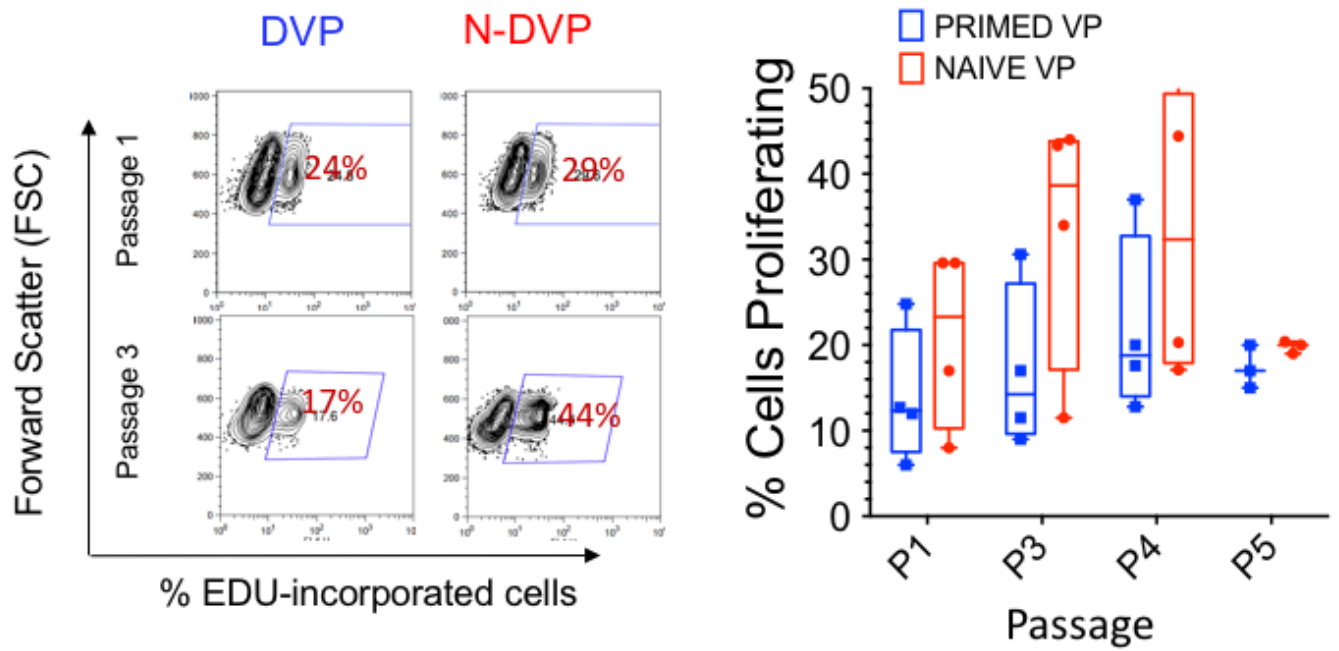
a



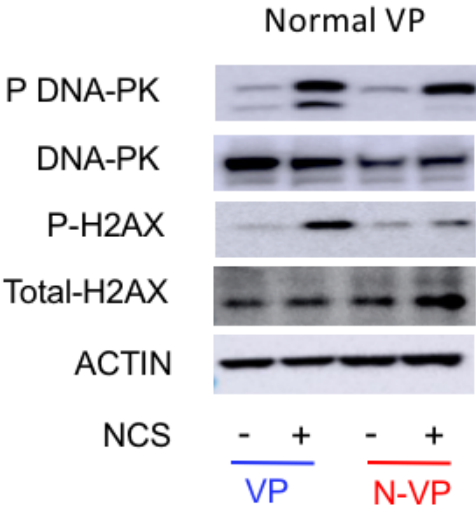
b



c

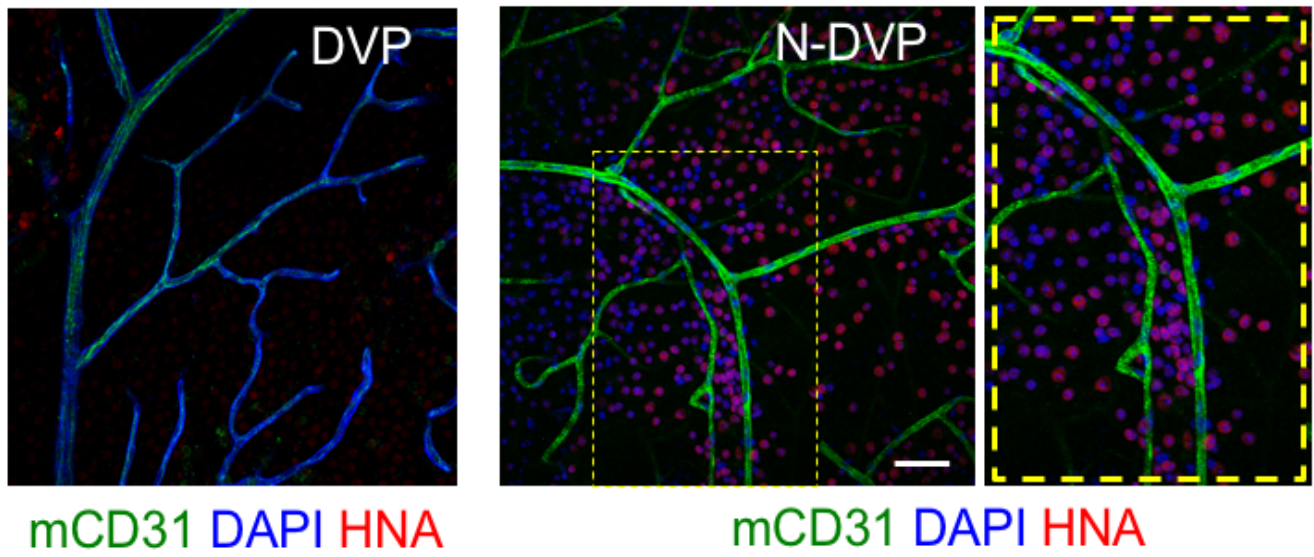


Supplementary Figure 6. Western blot analysis of DNA damage response (DDR) proteins following treatment of primed VP and N-VP with NCS. Purified and replated VP vs N-VP differentiated from isogenic primed normal fibroblast-hiPSC (C2); with (+) and without (-) NCS treatment prior cell lysate collection. P-DNA-PK: phosphorylated DNA-PK; P-H2AX: phosphorylated H2AX; NCS: neocarzinostatin.

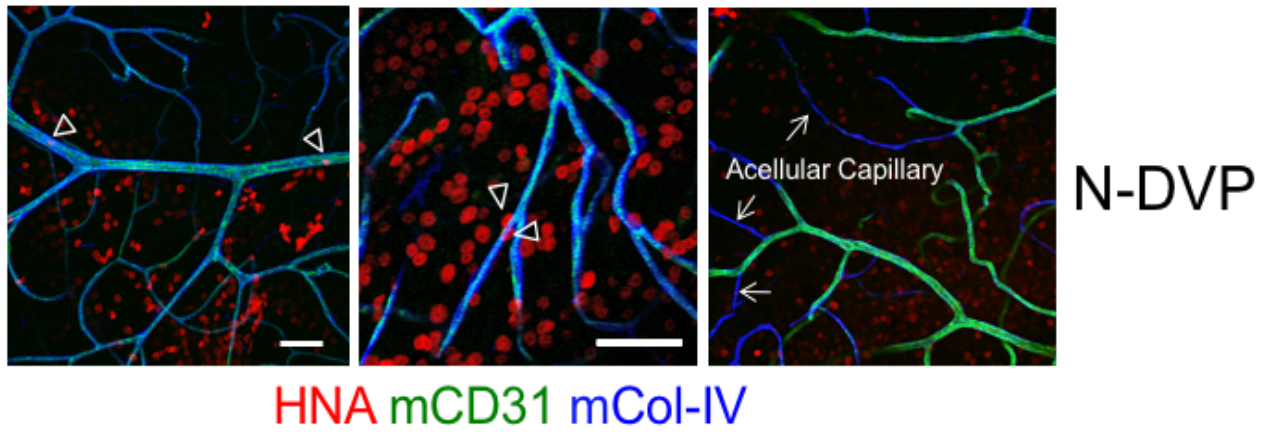


Supplementary Figure 7. Human VP cell therapy of murine ischemic retinopathy following I/R injury. Representative high magnification images from whole mount retinae demonstrating more abundant survival of HNA⁺ N-DVP cells in the superficial vascular layers of the retina relative to primed DVP at (a) 7 days and (b) three weeks following parallel intra-vitreous injections of 50,000 DVP or N-DVP cells per eye. (b) Retinal vascular regions at 3 weeks demonstrated that HNA⁺ human DVP cells were located either abundantly in suspension within vitreous or had migrated and engrafted into vascular abluminal regions of murine ischemic vessels (arrow heads). Scale bars = 50 μ m. Whole mount retinae were also stained with anti- murine CD31 (mCD31) or anti-murine collagen IV (mColIV) antibodies for maximum-intensity projection imaging. (c,d) Human vascular engraftment of murine retinae at 2 weeks post DVP injection. (c) Whole mount retinal staining of mouse CD31 (mCD31) and co-staining with murine collagen type-IV (mCol-IV) at 2 weeks following I/R injury and naïve (N-DVP) injections; (d) co-staining with human CD34 (hCD34)-specific and murine collagen type-IV (mCol-IV) antibodies of similar whole mount retinal samples demonstrated that a subset of these mCD31⁺mCol⁺ murine vessels had engrafted CD34⁺ vascular cells.

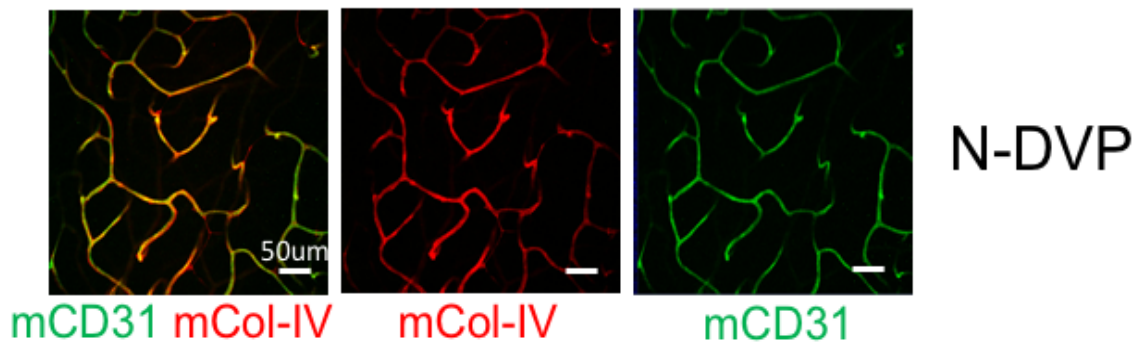
a



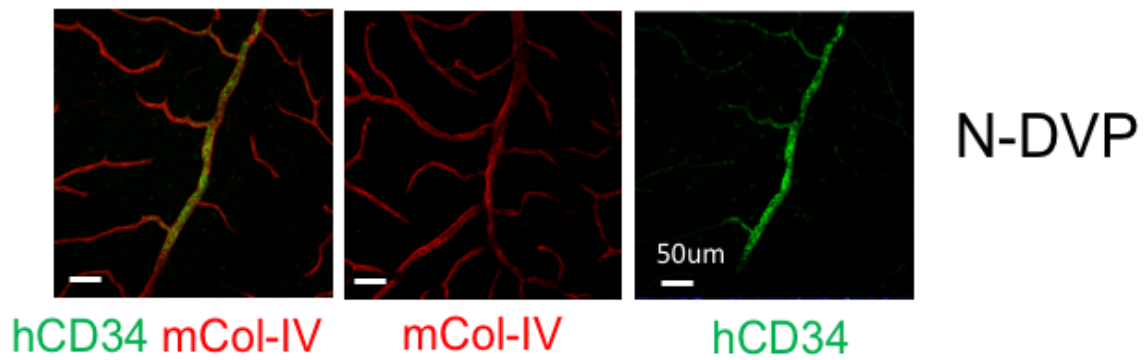
b



c

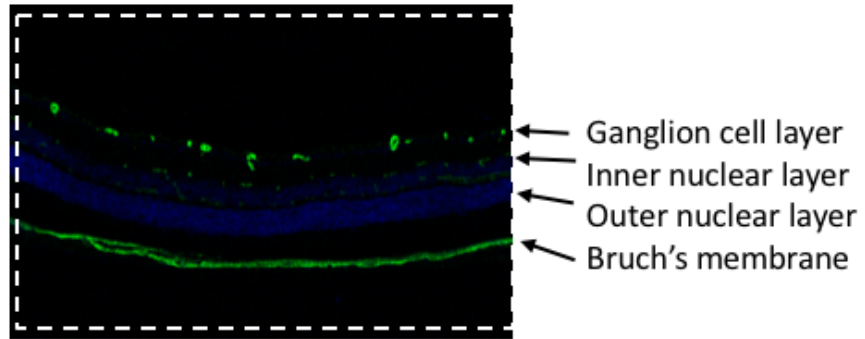
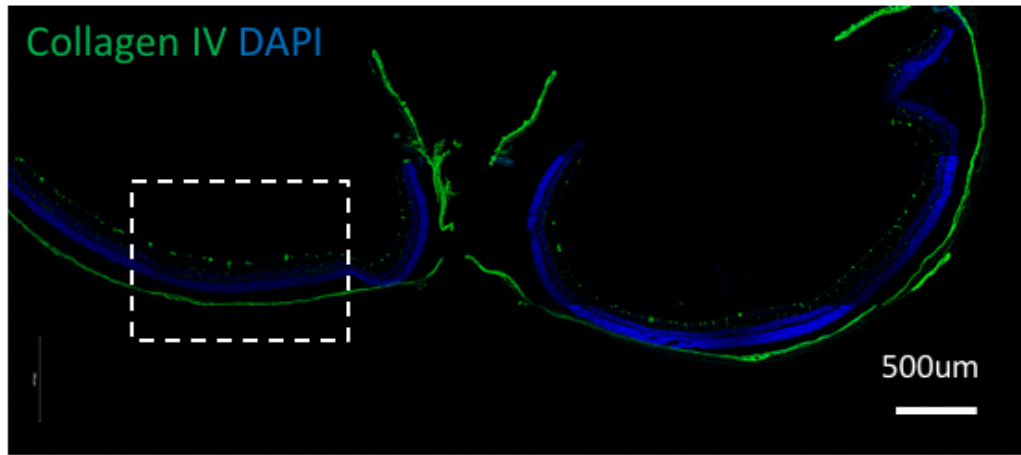


d

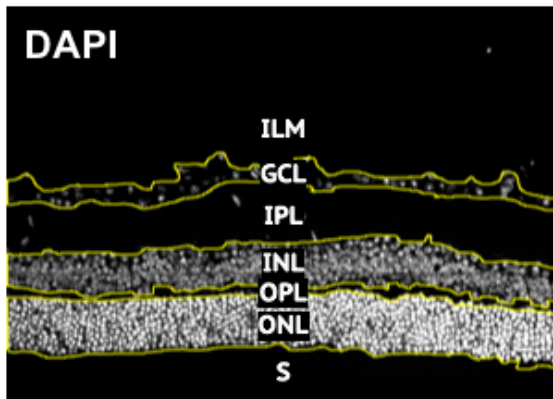


Supplementary Figure 8. Method of quantitating human DVP cell engraftment in the vasculature of the neural layers of ischemia-injured mouse retinae. (a) Tile-scanned image of cryo-sectioned retina. Multiple images were taken in 20x magnification from each cryo-sections as well as spaced (serial sectioned) retina sections for quantification studies. Hatched areas demonstrate representative example of neural retinal regions evaluated for human vascularization of murine blood vessels. (b) Method of regional separation of neural retinal layers employed for quantification of human CD34⁺ cells (hCD34) for data presented in **Figure 7b** and **7d** via automated counts using Fiji distribution of ImageJ software, as described in Methods.

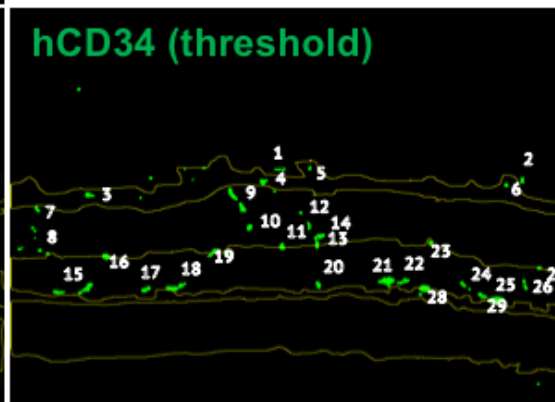
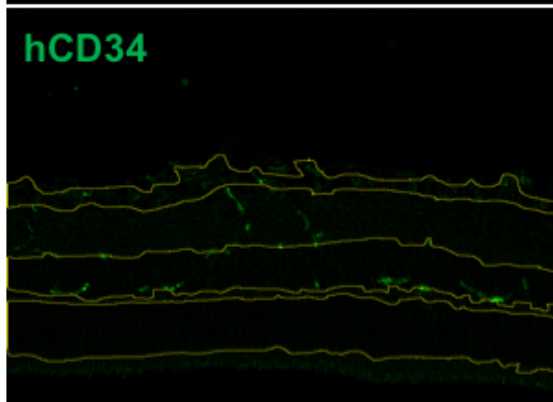
a



b

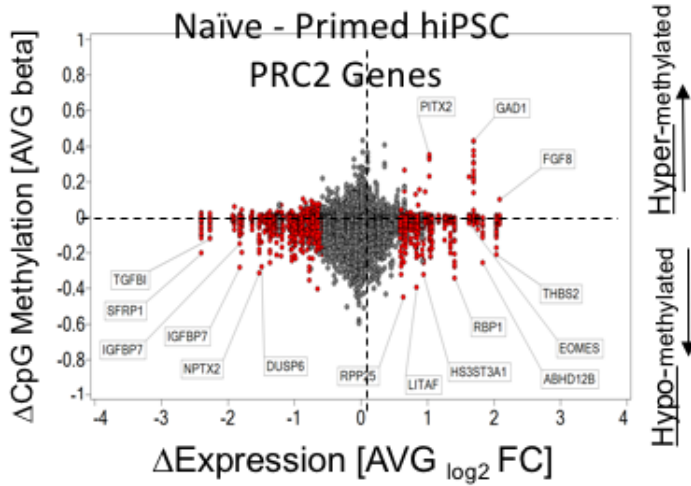


inner limiting membrane	ILM
ganglion cell layer	GCL
inner plexiform layer	IPL
inner nuclear layer	INL
outer plexiform layer	OPL
outer nuclear layer	ONL
segments	S

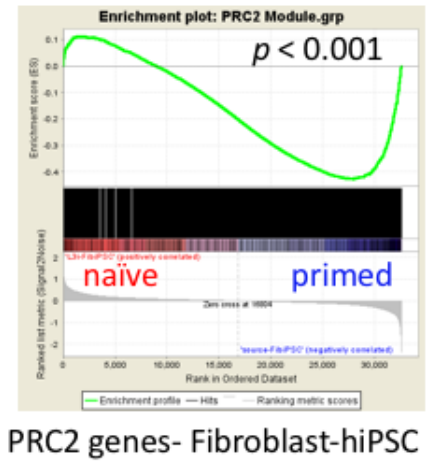


Supplementary Figure 9. Lineage-primed gene expression and epigenetic configurations of PRC2-regulated bivalent promoters in primed vs naïve DhiPSC. (a) Crossplot of mean genome-wide gene expression of PRC2 module gene targets (**Supplementary Table 3**) vs. CpG methylation of non-diabetic N-hiPSC vs. their isogenic primed isogenic hiPSC counterparts ($n=6$ normal hiPSC lines; **Table S1**). Plotted are the differentially methylated region (DMR) CpG methylation beta values of PRC2 module promoter regions in LIF-3i-reverted hiPSC minus their isogenic primed hPSC counterparts (y-axis, $p \leq 0.05$) vs. their corresponding differential gene expressions for the same genes (red, x-axis, \log_2 fold changes (FC); $p \leq 0.05$, FC +/- ≥ 1.5). (b) Curated GSEA pathways for gene targets of the PRC2 module over-represented (FDR <0.01 ; $p<0.001$) in LIF-3i-reverted fibroblast-hiPSC vs. their isogenic primed counterparts ($n=4$; normal hiPSC lines – **Supplementary Table 1**). (c) Comparison of differentially expressed ($p \leq 0.05$, fold change (FC) +/- ≥ 1.5) lineage-primed transcriptional targets of the PRC2 module (**Supplementary Table 3**) in naïve vs primed hiPSC ($n=6$ independent lines). FC: normalized ratios of naïve/primed expression microarray signal intensities show broadly decreased expressions of PRC2 targets in N-hiPSC lines. Ratios are of LIF-3i-reverted vs. primed hPSC samples. (d) ChiP-qPCR for H3K27me3 and H3K4me3 histone marks at key multi-lineage developmental promoters in primed vs N-DhiPSC line E1C1. Data is presented as percent input materials between naïve and primed D-hiPSC line E1C1. Standard error of the mean (SEM) bar represents replicates. ChiP-PCR primer sequences and sources are detailed in **Supplementary Table 3**.

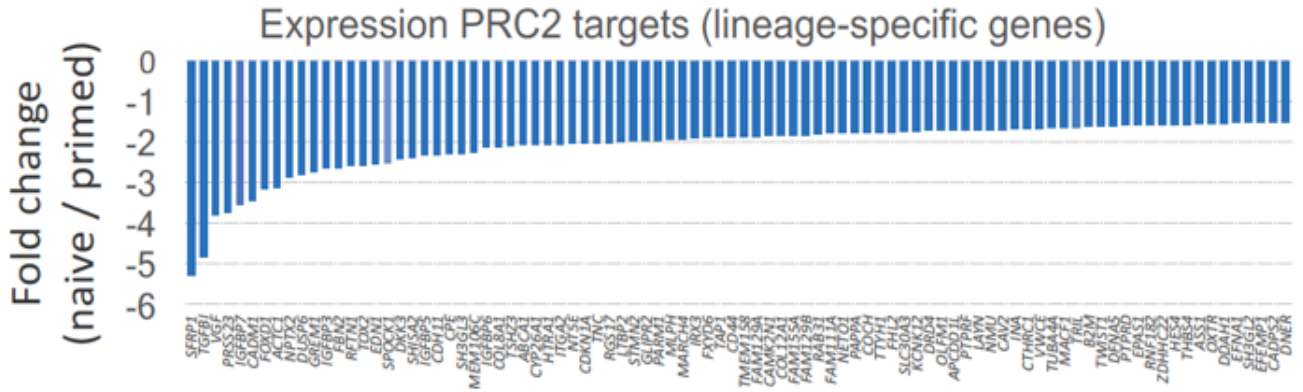
a



b



c



d

